POLITECNICO DI TORINO
Repository ISTITUZIONALE

A DBSCAN-based automated operational modal analysis algorithm for bridge monitoring

(Article begins on next page)

25 April 2024
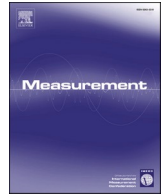
A DBSCAN-based automated operational modal analysis algorithm for bridge monitoring

Marco Civera [a,*], Luigi Sibille [b], Luca Zanotti Fragonara [c], Rosario Ceravolo [a]

[a] Department of Structural, Building and Geotechnical Engineering, Politecnico di Torino, 10129 Turin, Italy
[b] Department of Ocean Operations and Civil Engineering, Norwegian University of Science and Technology (NTNU), 6009 Ålesund, Norway
[c] School of Aerospace, Transport and Manufacturing, Cranfield University, Cranfield, Bedford MK43 0AL, UK

ARTICLE INFO

ABSTRACT

Advanced data analysis techniques are of paramount importance for the Structural Health Monitoring (SHM) of civil buildings and infrastructures. In particular, Automated Operational Modal Analysis (AOMA) algorithms are necessary for the output-only monitoring of such massive and large structures. The unsupervised estimation of their modal parameters from ambient vibrations enables assessing their integrity efficiently and continuously. This is particularly important for reinforced concrete (RC) bridges, which need constant maintenance. In this context, the classic cluster-based, multi-stage approach is effective in cleaning the stabilisation diagram and discerning stable and unstable modes. However, due to the shortcomings of binary classification with ($k = 2$)-means clustering, the labelling between 'possibly physical' and 'certainly spurious' modes may not be completely reliable. The procedure described here applies Density-Based Spatial Clustering of Applications with Noise (DBSCAN) to bypass this limitation. This allows, among other advantages, to automatically detect and remove outliers, differently from the traditional techniques. The algorithm is fully automated, including the data-driven setting of DBSCAN parameters. Its viability is tested here on a real, full-scale case study, the Z24 road bridge dataset.

1. Introduction

Bridges and transport infrastructures are one of the most important factors for the well-functioning of a country's economic activities. During their long-lasting service time, civil infrastructures should meet safety and reliability requirements accounting for continuous traffic loads and extreme environmental conditions such as floods, earthquakes, storms, etc. Yet, since the number of aged and damaged infrastructures is consistently increasing over the years, their constant monitoring is of paramount importance. In the last years, rapid advancements in sensor technologies led to the development of robust and efficient Structural Health Monitoring (SHM) techniques based on vibrational measurements [1–3], acoustic emission [4], fiber optic sensors [5,6], etc. However, despite these important achievements and progresses in SHM systems, some challenges (e.g., measurement errors, the ability to detect the changes with high level of confidence, the dependence on sensor and storage system, the reliability and validation of the results, etc.) are still matter of discussion and further research is needed.

Most vibration-based techniques rely on System Identification (SI) methods. Indeed, in many standard applications, SHM often reduces to tracking the identified modes of vibration in the time, frequency, or joint time–frequency domain. According to the classic Statistical Pattern Recognition framework, any substantial deviation from the expected behaviour could be linked to the occurrence of damage.

This is the basis of Vibration-Based Inspection (VBI). Indeed, vibrational signal processing has been extensively proven as a viable tool for damage detection in many applications, ranging from leak detection in pipelines [7,8] to fault detection in electric machines [9] and asynchronous motors [10]. For mechanical and aerospace applications, generally, the needed dynamic tests can be done in controlled environments, e.g. during laboratory experiments, where both the excitation and the output signals are simultaneously recorded. Instead, only the output response is available for most civil engineering purposes, given that is not possible to excite massive structures such as large multi-span road bridges. For this reason, Ambient Vibration (AV) tests and output-only SI are widely applied. This framework is conventionally referred to

Nomenclature

f_s	sampling frequency
i	number of block rows in the data Hankel matrix
j	number of block columns of the same
n	model order, corresponding to the number of poles identified
l_n	number of poles belonging to the n-th model order
λ_p	eigenvalue of the generic p-th pole.
f_p	natural frequency of the same
ξ_p	damping ratio of the same
$\boldsymbol{\varphi_p}$	array representing the mode shape of the same
$\nu = 1 - MAC(\boldsymbol{\varphi_p}, \boldsymbol{\varphi_q})$	complementary of the Modal Assurance Criterion defined between $\boldsymbol{\varphi_p}$ and $\boldsymbol{\varphi_q}$
$\boldsymbol{d_p^n}$	array of distances between the p-th pole of the n-th model order and all the poles of the following model order $(n+2)$
$\Delta\lambda, \Delta f, \Delta\xi, \Delta MPD$	absolute difference between the eigenvalues/natural frequencies/damping ratios/Mean Phase Deviation of the p-th pole of the n-th model order and the closest

	neighbouring q-th pole of the following model order $(n+2)$
$\Delta\boldsymbol{\lambda^n}$, etc	array of the absolute differences for each pole of the n-th model order
$\Delta\boldsymbol{\lambda}$, etc	array of the absolute differences for each pole of each model order
γ	parameter for the Box-Cox transformation
$\boldsymbol{h}$	Box-Cox transformation of $\Delta\lambda, \Delta f, \Delta\boldsymbol{\xi}, \Delta\boldsymbol{MPD}$, and $\boldsymbol{\nu}$
μ	mean of $\boldsymbol{h}$
σ	standard deviation of the same.
z	z-score of the values of $\boldsymbol{h}$
k	number of means for the k-means clustering
$\tilde{d}$	distance threshold for hierarchical clustering (dendrogram cut-off)
$Sil(p)$	Silhouette value of the generic p-th pole
$MinPts$	minimum number of points required to form a dense cluster in DBSCAN
ε	search distance around a point in DBSCAN
κ	κ-distance graph for DBSCAN

as Operational Modal Analysis (OMA) and can be applied to basically any typology of road, rail, or pedestrian bridge – see e.g. [11] and [12] for concrete deck superstructures supported by steel girders, [13,14] and [15] for cable-stayed bridges, [16] for masonry arch bridges, [17] for concrete arch bridges, and [18] for prestressed multi-span concrete bridges.

The remainder of this paper is organised as follows. Section 2 describes the theoretical background of this research study. In Section 3, the main aspects of the complete AOMA algorithm in general, and of the DBSCAN-based step in particular, are reported. Section 4 describes the case study of interest. Section 5 details, step-by-step, the application of the AOMA algorithm to the Z24 dataset, showing the intermediate and final results. A comparison with the identifications from the authors of the original dataset is included as well, for direct comparability. Finally, the Conclusions (Section 6) end this paper.

2. Theoretical background

2.1. Current state of OMA and AOMA procedures

The main issues for OMA are that

I. the number of relevant vibration modes is not known a priori;
II. the input AV force has a very low amplitude, so many modes are weakly excited;
III. output-only recordings from AV tests are noisy.

Due to point (I), the common strategy is to perform SI with many model orders, starting from a low value $n = n_{min}$ and increasing over an arbitrary range up to a given $n = n_{max}$. This approach leads to a large set of identifications, which need to be properly interpreted. In fact, this strategy is purposely intended to err on the side of safety.

On the one hand, the overestimated model orders are more likely to identify even weakly excited modes. This solves the issue of point (II). On the other hand, with noisy data, spurious modes arise due to several reasons (characteristics of excitation, measurement inaccuracies, etc) unrelated to the physics of the target structure.

The interpretation of the results is generally accomplished through a stabilisation diagram [19], plotting the identified natural frequencies and damping ratios vs. the model orders. The rationale is simple: stable modes – i.e. the ones recurring in most of the model orders with almost unchanged parameters – are more likely to be physically meaningful,

while randomly distributed identifications are, conversely, most likely noise-induced.

Thus, the main aim of Automated OMA (AOMA) is to perform the clearing and interpretation of the stabilisation diagram in an unsupervised fashion, taking all the identified poles in input and providing the extracted modes in output without manual user interaction.

In this regard, the classic procedure was clearly defined in [20], with a multi-stage clustering approach. Their proposed approach consists of [20]:

1. Single-pole validation criteria;
2. Clustering and cluster-wide validation criteria;
3. Estimation of the modal parameters representative of each remaining cluster.

This 3-step process is nowadays widely accepted by the SI and SHM communities. The number and relevance of AOMA applications that follow it have multiplied over the years, including examples of implementations for the permanent monitoring of complex structures [21]. The same framework has been then further developed and improved by many authors in the following years. Some examples include the works of [22] and [23].

Departing from the complete set of identified poles, all these algorithms firstly apply the single-mode criteria. These are intended to determine if a particular pole is certainly spurious or not. This is achieved by utilising Hard and Soft Validation Criteria (HVC and SVC, respectively). HVC yield, by definition, to a binary answer (e.g. stable or not) and are generally defined a priori, according to first principles. SVC, on the other hand, return a continuous range of values [20]. Therefore, a threshold must be defined, separating the poles between the two groups – likely mathematical from likely physical. This thresholding is conveniently data-driven, to adapt to the case study of interest.

HVC and SVC are commonly deemed as efficient in the current scientific and technical literature; overall, they have been applied for almost a decade with few changes (mainly regarding the proper selection of features for SVC, as investigated by [22]).

The second step of the procedure (clustering and cluster validation criteria) is, however, more prone to practical issues – mainly, the risk of labelling some remaining misidentified spurious poles as physically meaningful.

Indeed, after HVC and SVC, all the poles that, on their own, were deemed stable (and thus not obviously mathematical) are stored.

Nevertheless, as said, these remaining poles are in large part still spurious. To identify and discard them, the solution envisioned by [20] and followed by most researchers is a second sifting step. The idea is that densely and more populated clusters are most likely related to physical modes that are ideally identified at each model order from a certain model order forward. In contrast, sparsely and less populated clusters are expected, with good confidence, to be made up of spurious modes.

2.2. Problem statement

Clustering and cluster-wide classification are generally performed by (agglomerative) hierarchical clustering, followed by a binary classification between less and more populated clusters. In the original framework of [20], this binary classification is performed by means of $(k = 2)$-means clustering.

However, this approach (hierarchical clustering plus binary classification) presents three well-known shortcomings:

   I. It focuses on cluster population rather than cluster population density;
  II. The k-means algorithm is known to be biased to split the feature domain into (here, $k = 2$) sets of mostly equal size [22,24];
 III. It only deals with clusters of spurious poles and not with the single mathematical poles closer to the physical ones.

The issue of point (I) regards the distinction between weakly excited and spurious modes. As mentioned, this is the most compelling issue in the current AOMA state of the art. Weakly excited modes tend to be identifiable only at high model orders; thus, they form clusters with relatively low population, but generally high density (as they remain stable for higher model orders). On the other hand, spurious modes occupy all the space in the feature domain between actual (physical) modes. If a large enough region is considered, this may result in a cluster with very low density yet enough poles to have a larger population than weakly excited modes' clusters.

The issue of point (II) concerns how, in the standard AOMA procedure, the k-means-based binary classification works. Basically, it defines a 'Certainly Mathematical' (CM) centroid and its 'Possibly/ Probably Physical' (PP) counterpart [22]. The distance between these two points in the multi-dimensional feature space of interest is then computed. Whichever cluster is closer to one centroid than to the other is included in that group.

This implies that any cluster (even slightly) closer to the PP centroid should be physical. However, it was proved in previous studies [16] that clusters much closer to the PP centroid than to the CM one can still be spurious, as there is no guarantee that the boundary between these two regions necessarily falls exactly halfway. In many applications, this can lead to misidentifying CM clusters as PP clusters or (unlikely) vice versa.

Importantly, it must be remarked that 2-means clustering is already applied in the SVC phase, to classify the single poles as stable or unstable and discard the latter. This first use suffers from the same issue – a tendency to overestimate the number of stable poles, as they generally are much less than the unstable ones. Yet, this issue is not critical since the sifting at the single pole level is then followed by further selection at the cluster level. That is to say, the redundancy of the multi-stage procedure allows for some tolerance in the earlier stages.

Point (III) reports the final (and relatively minor) disadvantage of the classic approach. The spurious poles that are far from their peers but close to PP poles end up being included in their nearby clusters. Thus, they remain as outliers in a cluster otherwise made entirely of legitimate identifications. Hence, they need to be further removed in a subsequent, distinct step, as e.g. described in the section 3.6 of Neu et al. [22]. Otherwise, they can skew the modal parameters estimated from the corresponding cluster.

In conclusion, the AOMA procedure applied and discussed here is intended to retain the best practices introduced by [20,22] and in

previous research works, while dealing with the aforementioned issues.

2.3. The proposed DBSCAN-based procedure

The AOMA algorithm described here replaces the hierarchical and k-means clustering with a density-based clustering strategy. In particular, the Density-Based Spatial Clustering of Applications with Noise (DBSCAN, [25]) is utilised. DBSCAN was already applied, in a different fashion, for Operational Modal Analysis by Tronci et al. [26]. The main difference with that work is that the approach presented here is completely data-driven, including for the definition of the DBSCAN parameters, thanks to the use of a heuristic method and a clustering evaluation index.

This DBSCAN-based procedure is intended to perform a threefold task:

   I. the clustering of the poles remaining in the cleansed stabilisation diagram;
  II. the removal of the clusters entirely made by mathematical poles;
 III. the removal of outliers close to the remaining PP clusters.

As it will be shown, not only DBSCAN can incorporate these three stages in a single step but it is also not affected by the aforementioned typical issues of k-means clustering. Indeed, the main difference between DBSCAN and other more classic algorithms is that mathematical poles are directly identified as noise and discarded in the clustering phase. Besides, this approach results to be a less complicated and faster alternative than the conventional approach (as it will be shown in the presented case study).

However, DBSCAN needs to specify two parameters that are usually estimated manually accordingly with the distribution of points and the quantity of noise. As mentioned, in the proposed algorithm this selection is instead data-driven and fully automated.

The Z24 [27], one of the most renowned case studies in bridge monitoring, is used as an example. It will be shown

  (i) how the algorithm can correctly identify the modal parameters of the target structure under changing environmental conditions and levels of damage, and
  (ii) how these estimations can be used for vibration-based damage assessment, according to the most classic approach of following the downward frequency shift.

3. Methodology

As mentioned in the previous sections, the AOMA procedure described here mainly follows the multi-staged framework described by [20]. Indeed, many aspects of the AOMA implementations by [20] and [22] were previously tested and validated in [23]. All the components of these algorithms that were deemed as already efficient and optimised were thus retained for this work as well. These will be recalled here to make this discussion self-sustained; however, the reader is redirected to the respective references for further technical details, as well as for the theoretical and practical justification of each step. Only the main differences from these references will be highlighted and thoroughly commented upon. Particularly, the focus will be on the main novelty i.e. the inclusion of the Density-Based Spatial Clustering of Applications with Noise (DBSCAN) in the overall process.

3.1. Recalls on SSI

The Stochastic Subspace Identification (SSI) algorithm is considered among the best and most used techniques for output-only identification – see e.g. [28]. A detailed discussion can be found in the book of Van Overschee & De Moor [29].

Four parameters are required for SSI: the number of block rows (i)

and block columns (j) in the Hankel matrix, the minimum order model (n_{min}), and the maximum one (n_{max}).

Regarding j, this is conventionally set as:

$$j = s - 2i + 1 \tag{1}$$

for s data samples. Conversely, there is no agreed-upon formulation for i, as many textbooks report slightly different 'rules of thumb' for this purpose. For reasons specified in [23], here

$$i = f_s/2 \tag{2}$$

is considered, where f_s is the sampling frequency. Eq. (2) is equivalent to the formulation proposed by [30] assuming the first natural frequency of the inspected structure to be 1 Hz. As it will be shown in the results, this assumption does not hold true for the application (where $f_0 \cong 4$ Hz); yet, it errs on the side of caution.

Regarding the range of model orders $n_{min} - n_{max}$, its optimisation is still a matter of research, not yet totally solved. Some considerations in this regard can be found in [23] and [16]. For this specific application, $n_{min} = 10$ and $n_{max} = 160$ are considered, also for consistency with the same case study as investigated in [20]. For convention, the model order corresponds to the number of identified poles. Being these poles all complex conjugate pairs (as will be seen in the next subsection), n is increased in steps of two ($n_{min}, n_{min} + 2, \cdots, n_{max}$).

3.2. Hard validation criteria (HVC)

Due to their importance, the Hard and Soft Validation Criteria are here described in detail.

For the HVC, the criteria suggested by [20] were retained:

$$0\% \leq \xi_p \leq 20\% \tag{3}$$

$$Re(\lambda_p) \leq 0 \tag{4}$$

$$Im(\lambda_p) \neq 0 \tag{5}$$

For each p-th pole of any n-th model order, where ξ_p is its corresponding damping ratio and λ_p its eigenvalue. The underlying assumption of Eq. (3) is that the viscous damping of real mechanics systems cannot physically be negative nor exceed very large values (set here at 20% in accordance with [31,32]). Eq. (4) and (5) restrict the research to decaying oscillations only, for obvious reasons.

3.3. Soft validation criteria (SVC)

Following the first sifting step, the aim of the SVC is to binary classify the remaining poles as stable or not. This requires a data-driven comparison between the identifications of different model orders. In this regard, the five comparison parameters suggested by [22] as the most statistically reliable are considered. These include the absolute difference between the eigenvalues

$$\Delta\lambda = |\lambda_p - \lambda_q| \tag{6}$$

the natural frequencies

$$\Delta f = |f_p - f_q| \tag{7}$$

and the damping ratios

$$\Delta\xi = |\xi_p - \xi_q| \tag{8}$$

In addition, two measures based on the mode shapes φ are employed: the Mean Phase Deviation

$$\Delta MPD = |MPD(\varphi_p) - MPD(\varphi_q)| \tag{9}$$

with $MPD(\varphi)$ as defined in [33], and the Modal Assurance Criterion, according to its classic definition [34]

$$MAC(\varphi_p, \varphi_q) = \frac{[\varphi_p^*\varphi_q]^2}{[\varphi_p^*\varphi_p][\varphi_q^*\varphi_q]} \tag{10}$$

Where * denotes the transposed conjugate vector. For all these parameters except the MAC, absolute (rather than relative) difference are employed, for reasons detailed in [23]. For the latter term, it is also set

$$\nu = 1 - MAC(\varphi_p, \varphi_q) \tag{11}$$

such that 0 indicates total similarity and 1 total dissimilarity.

Eqs. (6)–(9) and (11) are computed between each p-th pole of any n-th model order and a selected pole of the following $(n + 2)$-th model order. This selection can be done by minimising the distance

$$d_p^n = \Delta f_p^* + \nu_p \tag{12}$$

i.e. picking the 'neighbouring' pole q that satisfies

$$q = \text{argmin}(d_p^n) \tag{13}$$

where both Δf_p^* and ν_p are calculated between p and all the l_{n+2} poles identified with the model order $n + 2$ (l_{n+2} can be depurated from all the identifications discarded at the HVC step for computational efficiency). This results in two arrays of dimension $\Delta f_p^*, \nu_p \in \mathbb{R}^{1 \times l_{n+2}}$. The formulation of Δf_p^* is the same as of Eq. (7) but min–max normalised, for consistency with the other terms in ν_p (that is to say, it must be $\Delta f^* \in [0, 1]$).

Eq. (12) is a variation of the classic formulation

$$d_p^n = \Delta\lambda_p^* + \nu_p \tag{14}$$

proposed in [20]. The concept is to replace the complex-valued distance between eigenvalues with the real-valued distance between frequencies, as these latter ones can be generally identified more reliably (that is to say, they are not affected by the higher variability of damping estimates) [23].

Once the neighbouring pole q is selected, the vectors of comparison parameters can be defined (for each pole and each model order). By way of example, for $\Delta\lambda$, one obtains

$$\Delta\lambda^n = [\Delta\lambda_1^n, \Delta\lambda_2^n, \cdots, \Delta\lambda_p^n, \cdots, \Delta\lambda_{l_n}^n] \tag{15}$$

for all the poles identified with the model order n; concatenating all the vectors from all model orders into one array returns

$$\Delta\lambda = [\Delta\lambda^{n_{min}}, \Delta\lambda^{n_{min}+2}, \cdots \Delta\lambda^{n_{max}}] \tag{16}$$

The same process can be applied to the other four comparison parameters as well.

At this point, one could directly apply ($k = 2$)-means clustering to the 5-dimensional space defined by the terms of $\Delta\lambda$, Δf, $\Delta\xi$, ΔMPD, and ν, to classify stable and unstable modes. However, before doing so, a further intermediate step – recommended by [22] – is applied in the implementation proposed here.

In fact, k-means clustering assumes approximately normally distributed variables. Thus, a Box-Cox transformation [35] is used to enforce the statistical distribution of all comparison parameters to closely resemble a Gaussian model. Considering again $\Delta\lambda$ as an example, this can be obtained as.

$$h(\gamma) = \begin{cases} (\Delta\lambda - 1)/\gamma & \gamma \neq 0 \\ \ln\gamma & \gamma = 0 \end{cases} \tag{17}$$

where the parameter γ can be inferred by maximising the profile log-likelihood as described in [35]. Then, the resulting distribution h is standardised as

$$z = \frac{h - \mu}{\sigma} \tag{18}$$

where μ is the mean of h and σ is the standard deviation of the same. This guarantees that the z-scores in Eq. (18) are normally distributed as

$z \sim \mathcal{N}(0,1)$. As above, this process needs to be repeated for Δf, $\Delta \xi$, ΔMPD, and ν as well. The obtained arrays are then used for the second sifting step.

3.4. Density-Based clustering

As mentioned before, the HVC and SVC can be seen as single pole-level selection stages. In the classic approach proposed by [20] and followed (among others) by [22] and [23], the remaining poles would be firstly grouped through agglomerative hierarchical clustering. The principle of this approach is to obtain a nested sequence of clusters, where each pole is added sequentially to a hierarchical tree until they are all included in a single group. Thanks to a data-driven threshold, a cut-off distance is then defined and the dendrogram is stopped before unifying completely. Thus, a finite set of clusters (more than one) is defined.

At this step, the resulting clusters would be further sifted according to their population. ($k = 2$)-means clustering is applied again for this aim, returning two options: the aforementioned 'certainly spurious' and 'possibly physical' classes [20].

Instead, a non-parametric density-based clustering algorithm, the DBSCAN, is applied here. The main theoretical aspects of these two alternatives can be qualitatively compared as discussed in Table 1.

The rationale for the DBSCAN is that the clusters can be defined over dense, connected regions of data surrounded by less populated regions, inhabited only by outliers and noise. A detailed description of the DBSCAN algorithm can be found in the original works of [25]; in brief, the main steps are:

1. For each (still unlabelled) pole p in the identification's dataset, consider its ε-neighbourhood (i.e. the other poles that are included in a region of radius ε around it).
2. Density check: if at least *MinPts* poles (including p itself) are within this distance ε from it, define a new cluster C, label p as a *core point* of

C, and define all the other *MinPts* -1 poles as *directly reachable* from p. If not, label p as a *noise point*.
3. Expand the cluster C including all the poles that are (not directly) reachable from p. A pole q is said to be *reachable* if it exists at least one path of poles between p and q that are directly reachable from one another. Any pole between p and q is, by definition, a core point.
4. If q does not directly reach any other pole, label it as a *border point*.
5. When all paths arising from p end in a border point, move to the next unlabeled pole (if any remain).

Therefore, once all poles are labelled, these will necessarily be core points (the inside of each cluster), border points (its edge), or unreachable noise points/outliers.

3.5. Automatic (data-driven) setting of DBSCAN parameters

The main requirement for the user is the selection of the two input parameters, *MinPts* and ε. Noteworthy, if *MinPts* ≤ 2, DBSCAN will return the same results as hierarchical clustering (with the single link metric), considering a dendrogram cut at a height $\tilde{d} = \varepsilon$. Therefore, one must choose (at least) *MinPts* ≥ 3.

To make the proposed algorithm fully automated, a data-driven and data-adaptive strategy is here applied for these two settings.

3.5.1. Determination of MinPts via Silhouette index

MinPts represents the desired minimum cluster size. The general advice is to use higher values for noisy datasets and a lower threshold for clean and highly dense data. However, this profoundly affects the results and thus should not be left to the user arbitrariness but estimated from the data themselves. No specific guideline was found in the existing scientific literature for the aim of this setting in the specific field of dynamic System Identification. Thus, the procedure described hereinafter was tested. This relies on the Silhouette Index, a measurement described in [37] to evaluate the goodness of fit for clustering applications. Briefly, for each cluster, this can be defined by the ratio

$$Sil(p) = \frac{b(p) - av(p)}{\max(b(p) - av(p))} \tag{19}$$

where $b(p)$ is a measure of dissimilarity – defined in detail in [37] – calculated between the p-th pole and the closest pole of the same cluster. $av(p)$ is the average of the same measure computed for all the other poles in the same group. A good clustering will result in $Sil(p) \to 1 \; \forall p$ except for noise points. In fact, they are included in a distinct noise cluster, which encompasses all outliers. Since these are scattered throughout the whole $f - \xi - n$ space, their corresponding Silhouette values are all expected to be negative, meaning that they are closer to poles belonging to other clusters than to other elements of the same group (i.e. other outliers).

The iterative procedure can be then defined as follows:

1. Run DBSCAN with *MinPts* $= \lfloor N/5 \rfloor$ as a first attempt (where $\lfloor \; \rfloor$ indicates the floor function and N is the number of model orders considered between n_{min} and n_{max}.).
2. Perform the density-based clustering.
3. Compute, for each pole in each cluster, the Silhouette coefficients; then sum all values up.
4. Iterate steps 2 and 3, increasing *MinPts* until a maximum value of *MinPts* $= \lfloor N/3 \rfloor$ is reached.
5. Select *MinPts* according to the maximum value of Silhouette coefficients.

This proposed workflow requires several iterations, yet it takes advantage of the lower computational requirements of DBSCAN (this will be better discussed in the Results section). The lower limit for *MinPts*, defined in step 1, is generally higher than the minimum value suggested by [38] for generic uses, independently of the application

Table 1
Qualitative comparison of hierarchical and density-based clustering.

	Agglomerative hierarchical	DBSCAN
Working principle	The average linkage method [36] considers the distance between every point and every other point. It can return more or less densely populated clusters.	DBSCAN groups together closely-packed points, classifying them (for each cluster) as core points, border points, or (if not included in any cluster) noise data.
Required parameters	$\tilde{d}$: threshold distance between distinct poles.	ε: search distance around a point *MinPts*: minimum number of points required to form a density cluster
Advantages	The hierarchical representation can be very informative and easy to visualise. It can adapt to complex shapes (generally not needed here). It can discern non-linearly separable clusters (differently from k-means). It is more adapt when representing datasets that are actually hierarchically structured (not the case here). It does not require defining a priori the number of clusters.	It has built-in capabilities to recognise and discard noise and outliers.Can adapt to complex shapes (generally not needed here). It can discern non-linearly separable clusters (differently from k-means). It does not require defining a priori the number of clusters. It is computationally more efficient than hierarchical clustering (depends on ε but reaches $O(N^2)$ only in the worst case)
Disadvantages	It is particularly sensitive to noise and outliers. It is computationally intensive with run-time complexity of $O(N^2)$ for N data.	It faces difficulties in finding clusters with varying densities.

domain. In that work, it was suggested to consider at least *MinPts* = 2*D*, where *D* is the dimensionality of the space where the clustering is performed. However, the authors of the original algorithm explicitly state that "for datasets that have a lot of noise, that are very large, that are high dimensional, or that have many duplicates it may improve results to increase *MinPts*" [39]. The application for SI falls into these categories, especially due to the very large number of spurious modes. The maximum limit, on the other hand, is largely overestimated for precaution.

3.5.2. Determination of ε via elbow Rule.

ε can be set by using a κ-distance graph, plotting the distance to the κ nearest neighbours, ordered from the largest to the smallest value [39]. These will form a bi- or multi-linear distribution, with (at least one) pronounced 'elbow'. The corresponding value can be seen as an optimal setting for the search distance; this concept is known as the *elbow rule*.

Many authors – e.g. [38] – suggest using $\kappa = MinPts - 1$ for a given value of *MinPts*. However, this has two main limitations: (1) it is dependent on *MinPts*, thus requiring to be computed for each iteration; (2) due to the larger-than-usual values of *MinPts* applied in this domain, the suggested value of κ would be excessively high. It was proven in this application and similar previous applications [40] that $\kappa = 2$, i.e. the minimum possible, produced a clearly visible knee, leading to good

results, as will be discussed later in the Results.

3.6. Estimation of cluster-wide modal parameters.

Finally, the estimation of the modal parameters representative of each remaining cluster follows the recommendations of [16] and [23], assigning to each of them their mean values $\bar{f}$ and $\bar{\xi}$.

4. Case study: The Z24 road bridge

The case study of interest concerns a reinforced concrete (RC) road bridge, more specifically, a typical example of a post-tensioned concrete two-cell box-girder bridge [41]. This was located in the canton of Bern (Switzerland), between the municipalities of Utzenstorf and Koppigen, where the road overpassed the Bern-Zurich section of the A1 national highway. For brevity, only the main characteristics of the Z24 bridge, its sensor setup, and the experimental campaign will be recalled here. All the details about the structure and the monitoring system can be found in [41,42,43], and [27].

4.1. Bridge description

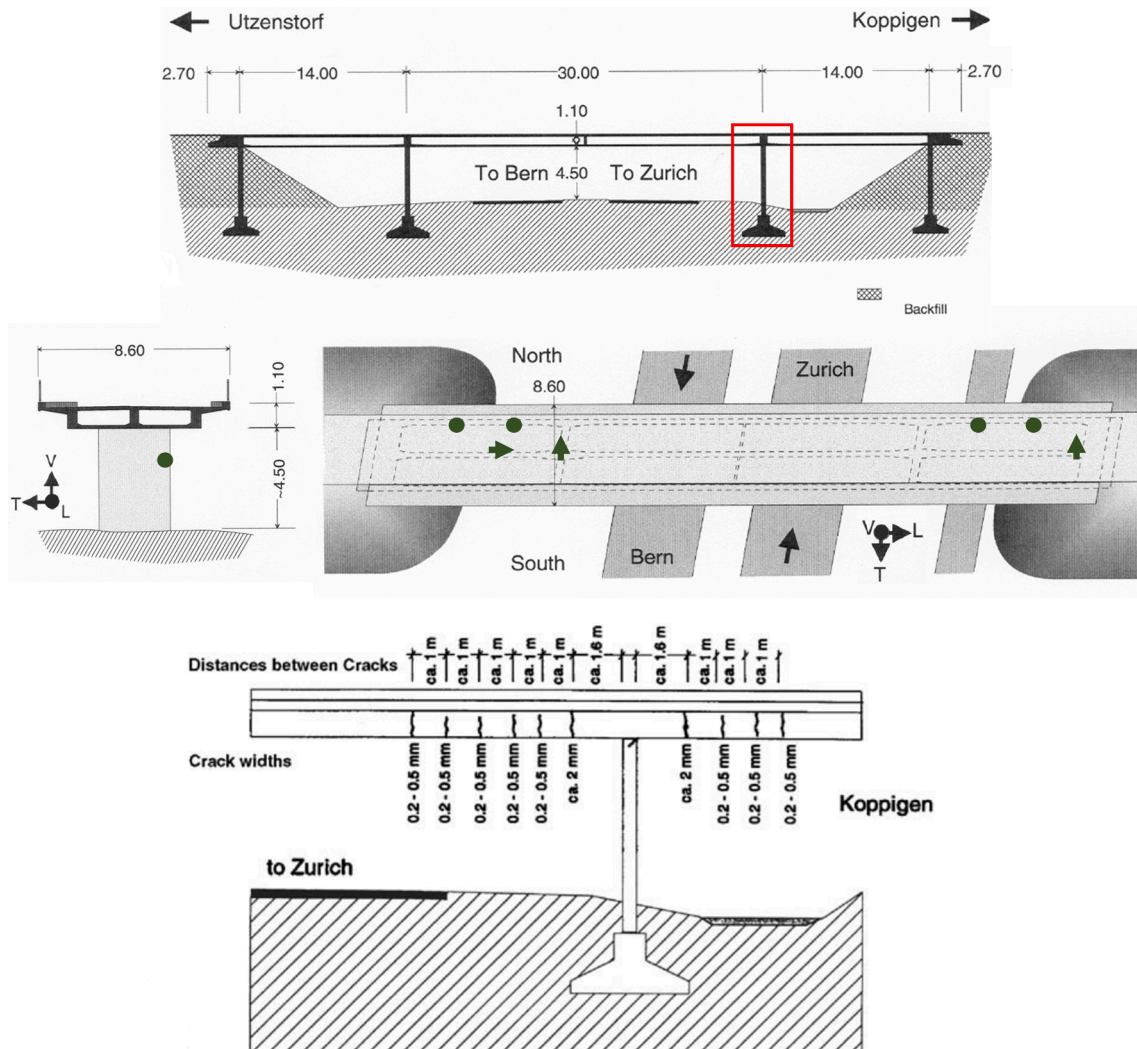The Z24 bridge (Fig. 1) consisted of three spans, a main (central) one

Fig. 1. The Z24 bridge case study. From top to bottom: frontal view (the red frame indicates the damaged pier); side and plan view; crack pattern. The green arrows indicate the sensors' location and direction. The global directions are longitudinal (L), transverse (T), and vertical (V) as shown in the reference frame. Adapted from [44] and [45]. (For interpretation of the references to colour in this figure legend, the reader is referred to the web version of this article.)

of 30 m and two side spans of 14 m. The two intermediate supports were made of concrete piers clamped into the girders, while both abutments consisted of two rows of three pinned concrete columns, again clamped into the girders [41]. The axes of the piers were not exactly perpendicular to the longitudinal girder axis, making the bridge slightly skewed (this generated some mixed bending-torsion vibrational modes to arise).

4.2. Experimental campaigns

The road bridge was deemed for demolition in 1997, due to the need for a larger side span for the new railway under construction parallelly to the A1 highway. Since the bridge had no known structural issues, it was decided to artificially introduce damage on its eastern pier (highlighted in red in Fig. 1), with incremental steps, to monitor the evolution of its vibrational response. Thus, the bridge was permanently monitored, with hourly recordings, for ten months, from 11 November 1997 to 11 September 1998 [41]. Thus, two phases were considered [46]:

I. From November till the end of July, the bridge was assumed to remain intact and unaltered, with no visible signs of changing structural conditions. This prolonged observation period allowed capturing many seasonal effects, especially freeze-induced deck stiffening, which affected noticeably the vibrational response of the target system.

II. The damage test procedure started in early August 1998 and led to the progressive lowering of the pier on the Koppinger side up to -95 mm (reached on 18 August 1998); this was intended to mimic erosion or subsoil settlement.

Other further damage scenarios were applied afterwards; these are detailed in [46]. Due to the inserted damage, the bridge was closed to traffic during the whole duration of the experimental campaign. In operating conditions, the presence of traffic loads would cause differences in the vibration amplitude and natural frequencies [47].

4.3. Experimental settings

The bridge was instrumented with many sensors reading the external temperature, humidity, wind speed etc. These are not recalled here since they are beyond the scope of this study. Of the 16 accelerometers originally deployed for long-term vibration inspection, only eight channels (marked by the green arrows in Fig. 1) survived for the whole duration of the permanent monitoring. The other accelerometers failed during the operation period. All the acquisitions included in the database are made up of 65,536 data points, with a sampling frequency $f_s = 100$ Hz and a duration of each acquisition equal to slightly less than 11′. A noteworthy aspect is that all measurements (a total of 5652 acquisitions corresponding, as mentioned, to ten months of hourly recordings [41]) accounted for over 6 Gb of data. These have been collected on a hard disk and then stored on 10 CDs after compression. Indeed, data storage is a relevant practical issue that can present a limitation to field applications. While not directly addressed in this article, this point will be the aim of future research works.

5. Guided example and results

The signals analysed with the AOMA procedure were obtained from the following acquisitions:

1. Acquisition 03B01, 24 November 1997, time 01:00, day 13
2. Acquisition 04G18, 06 December 1997, time 18:00, day 25
3. Acquisition 12E09, 29 January 1998, time 09:00, day 79
4. Acquisition 20D00, 25 March 1998, time 00:00, day 134
5. Acquisition 33E11, 25 June 1998, time 11:00, day 226
6. Acquisition 43A08, 30 August 1998, time 08:00, day 292

Th first five signals represent five instances before damage, corresponding to different weather and temperature conditions. The last (sixth) signal, Acquisition 43A08, corresponds to the post-damage conditions, specifically to the last day after the complete lowering of the pier (95 mm) and before the failure of the concrete hinge [46]. This induced the formation of the crack pattern depicted in Fig. 1 in the beam girder [45]. Thus, it is representative of the largest lowering-induced effects before the structural configuration of the bridge was modified irremediably.

All signals were pre-processed by detrending and lowpass filtering them with a cut-off frequency of 40 Hz. For conciseness, only the first one (Acquisition 03B01) will be detailed step-by-step in its intermediate results.

5.1. Step 0 – SSI

The SSI parameters were set as described previously in the Methodology section, leading to the identification of 3230 poles, represented in Fig. 2.a.

5.2. Step 1 – HVC

During the first sifting phase, 44 poles were removed due to negative damping values and 608 poles due to excessively high values ($\xi > 20\%$). No identification was found to have a null imaginary part. Hence, 2578 poles passed this step; these are portrayed in Fig. 2.b.

5.3. Step 2 – SVC

The distribution of stable and unstable poles for each pair of features, as obtained from the application of the k-means clustering, is described graphically in Fig. 3. Please note that, for all subplots on the lower left triangle, the distances along the x- and y-axes are expressed in terms of standard deviations due to the z-score standardisation (see [23] for a related discussion). Stable and unstable values are reported in red and in blue, respectively. The black crosses indicate the respective centroids. Since all the feature vectors have been transformed through the Box-Cox transformation, they closely resemble a normal distribution, so the resulting sets are approximately equal in size. The upper right triangle reports the corresponding correlation coefficients, while the distributions of the single features are on the main diagonal.

This second round of sifting resulted in 1236 poles deemed as stable (indicated by the red circles in Fig. 4). These were passed to the next stage, while the unstable poles (black crosses in Fig. 4) were discarded.

5.4. Step 3 – Application of DBSCAN

The DBSCAN parameters (*MinPts* and ε) were set according to the procedure discussed previously, finding *MinPts* $= 15$ and $\varepsilon = 0.0075$ for $\kappa = 2$. In this regard, Fig. 5 shows how considering larger values of κ-distance resulted in increasingly less pronounced elbows for equal *MinPts* and other settings. Overall, these alternatives proved to be less effective, causing multiple nearby modes to be included in a single cluster.

The corresponding Silhouette values are portrayed in Fig. 6.a. The label '-1′ corresponds to the outliers and noise points, dispersed in the $f - \xi - n$ domain surrounding the other clusters. The distribution along the identified clusters of the remaining poles is reported in Fig. 6.b. Finally, the resulting poles are reported in Fig. 7. The black ' × ' indicates the spurious poles (cluster -1), while the other poles are marked by '∘' (coloured accordingly to their group).

5.5. Step 4 – Estimate of cluster-wide modal parameters and final results.

The cleared stabilisation and order-frequency-damping ratio diagrams are depicted in Fig. 8. The poles shown there correspond to the
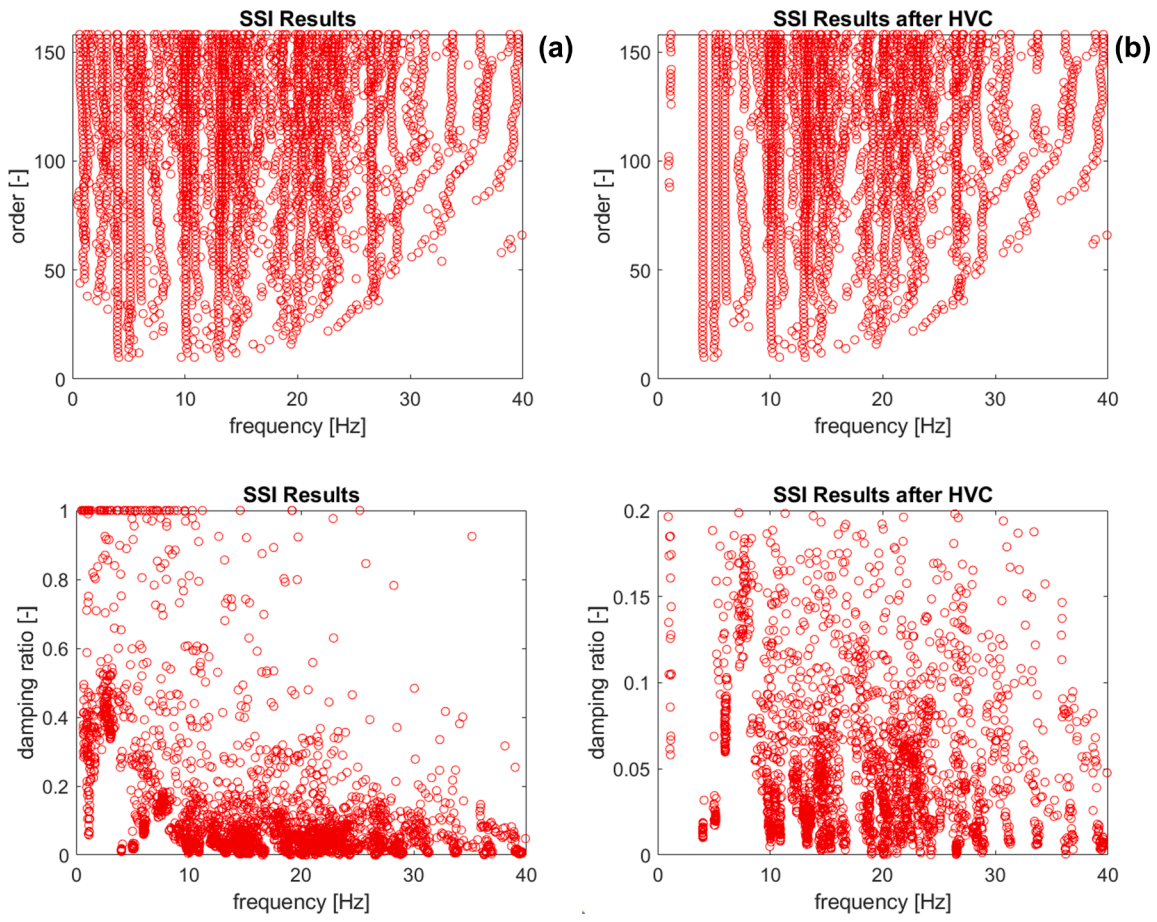
Fig. 2. (a) Poles identified from SSI. (b) Remaining poles after HVC. From top to bottom: stabilisation diagram and damping vs frequency diagram. Note that the range of damping values has been restricted to 0–0.2 for (b).
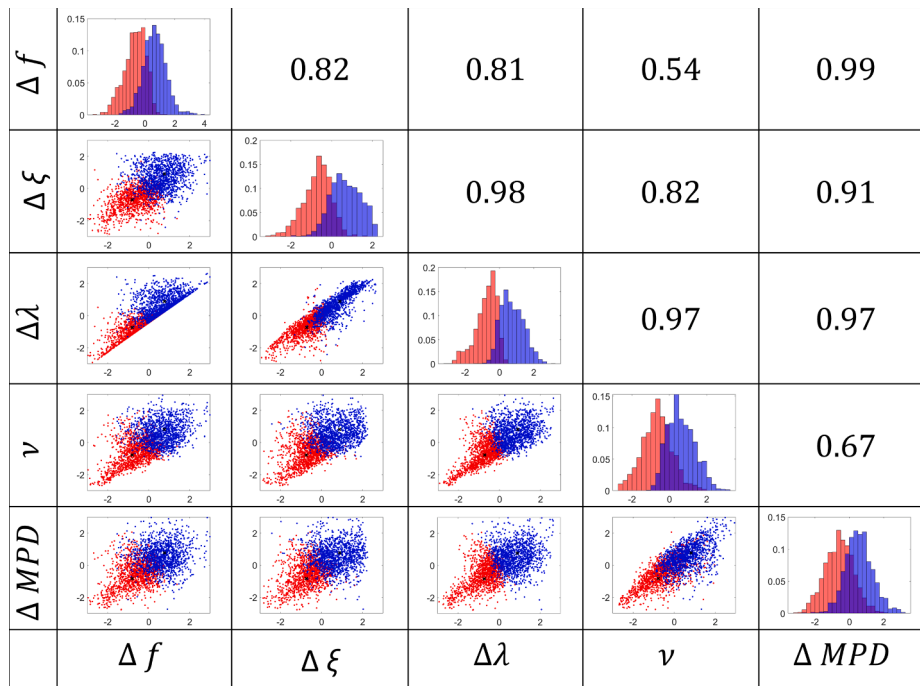

Fig. 3. The influence of the selection parameters on the 2-means 5-dimensional clustering process. Red: stable poles. Blue: unstable ones. (For interpretation of the references to colour in this figure legend, the reader is referred to the web version of this article.)
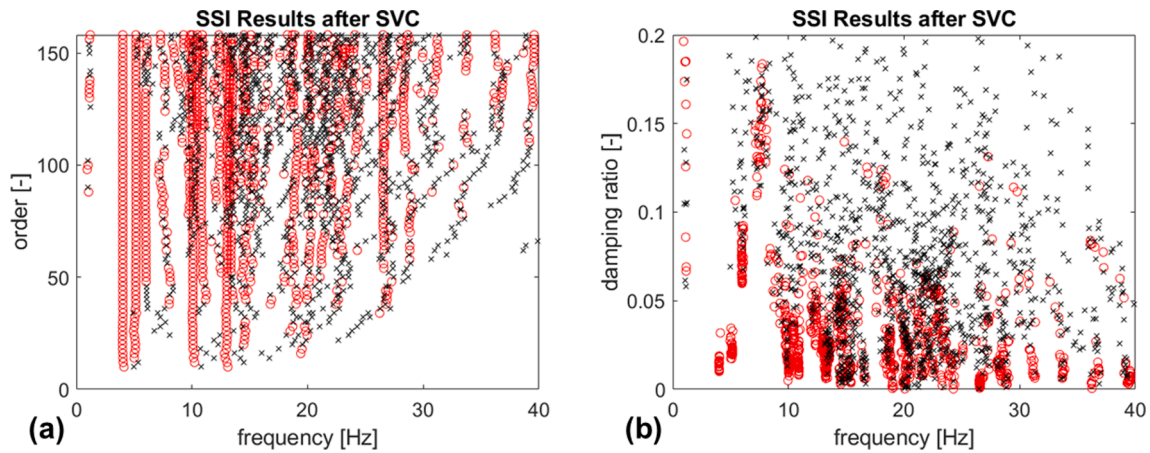
Fig. 4. Remaining poles after SVC. a) stabilisation diagram b) damping and frequency diagram.
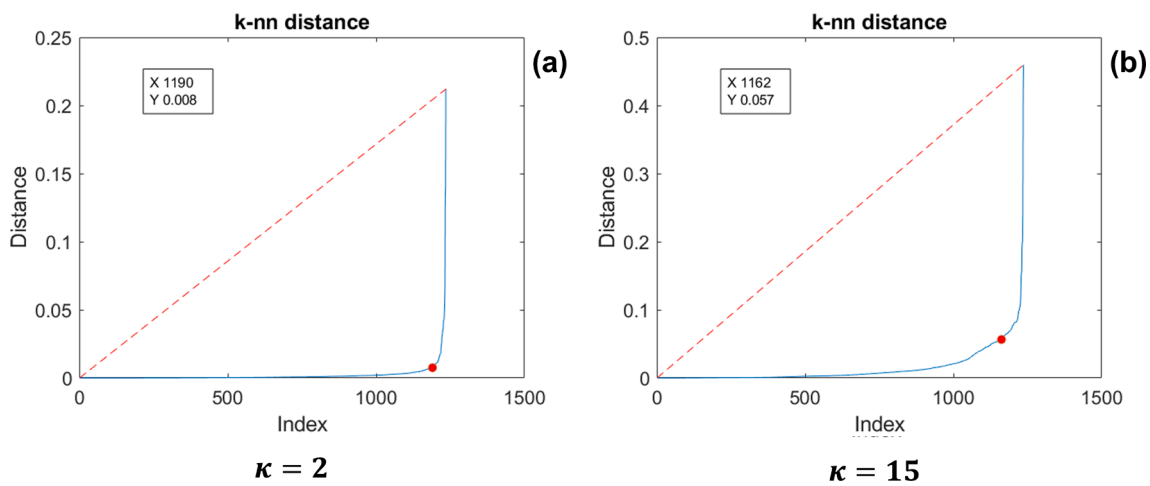

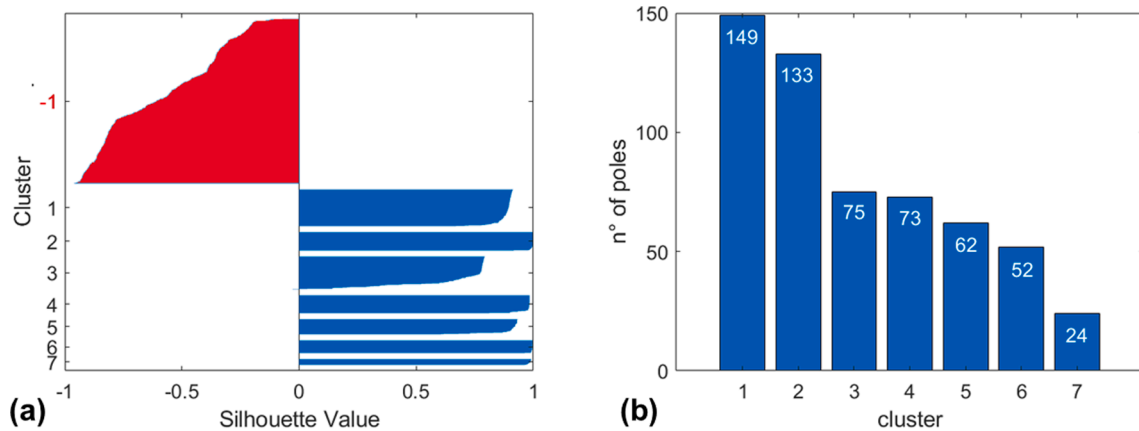**Fig. 5.** Two examples estimated values of ε for increasing κ: (a) κ = 2 and (b) κ = 15.

Fig. 6. (a) Silhouette values for the obtained clusters. (b) Cluster distribution of the poles deemed as physically meaningful.

modes enlisted in Table 2. Due to the position of the accelerometers (as seen in Fig. 1, only measurements from the side spans were available), the mode shapes could not be identified. Hence, only the eigen-frequencies and damping ratios were investigated. As said in the Methodology section, the mean natural frequency $\bar{f}$ and damping ratio $\bar{\xi}$ were deemed representative of their respective clusters.

For comparison, the values reported in [46] are included. Consider,

however, that these target values were obtained from a collection of 'shaker, ambient, and drop weight tests' (as stated in [46]); many of the modes reported there were not visible even in the raw data (i.e. in the SSI identifications) as extracted from AV tests only (specifically, acquisition 03B01). In fact, the use of a controlled input, while impractical, allows for better identification, especially of weakly-excited modes that are too small to be identifiable with small amplitude ambient vibrations.

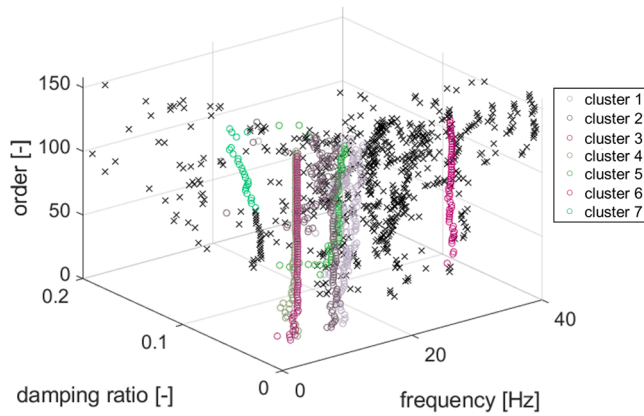Furthermore, the exact value of the natural frequencies is highly

Fig. 7. Poles labelled as physical (○) or spurious (×).

affected by the external temperature (this point as well will be discussed later in detail). Hence, without further information about the environmental and structural conditions, the comparison reported in Table 2 can be only considered qualitatively indicative.

The modes identified here are, nevertheless, comparable with the one presented in [20], which were extracted from AOMA identifications only (but related to the damaged scenario, as will be seen in the next section). Specifically, the first, second, and third bending modes were identified at $f_1 = 4.02$, $f_7 = 12.26$, and $f_8 = 13.20$ Hz, respectively. The higher bending modes, expected at $f_{11} \cong 19.7$ Hz and $f_{13} \cong 33.2$ Hz, were not identified, most probably due to their weaker excitation. However, these two modes are not mentioned in [20] as well. The first and the second lateral modes were encountered at $f_2 = 5.14$ Hz and $f_3 = 5.99$ Hz; the third one, expected at $f_4 \cong 8.4$ Hz, was not found. As before, the most probable explanation is that lateral modes are very weakly excited; [20] does not report either the 2nd or the 3rd lateral mode. $f_5 = 10.06$ Hz and $f_6 = 10.89$ Hz are two closely spaced mixed bending-torsion modes, caused by the slight skewness of the bridge supports [41]. Their identification was stated as particularly compelling in [46]. These two specific modes represent a relevant benchmark also for potential applications to other bridge structure types, e.g. cable-stayed bridges, that are notoriously subject to couplings between deck and cable modes as well as flexural–torsional modal coupling issues for specific complex geometries [48].

Finally, out of the four higher torsional modes (f_9, f_{10}, f_{12}, and f_{14}), only $f_{12} = 26.54$ Hz was identified. None of these higher modes is mentioned in [20].

5.6. Computational efficiency

For each iteration between $MinPts = \lfloor N/5 \rfloor$ and $MinPts = \lfloor N/3 \rfloor$, the DBSCAN algorithm run (on average) for 0.0046 ± 0.0028 s. The (agglomerative) hierarchical clustering, run on the same case study and stopped at the data-driven threshold, lasted 0.1847 s, i.e. several orders of magnitude slower (this includes three components: the definition of the agglomerative cluster tree, 0.0163 s, the definition of the threshold distance $\tilde{d}$, 0.1509 s, and the clustering itself, 0.0175 s).

Furthermore, when comparing the proposed algorithm to the classic procedure, one should consider that the DBSCAN (faster to run on its own) was iterated for increasing values to *MinPts*. However, for continuous monitoring, it is possible to run the estimation of *MinPts* only once. The optimised value can be then set and left untouched for future identifications on the same target structure. In this case, the procedure becomes slightly more efficient, with a total elapsed time of 16.40 s (averaged over 5 runs; in comparison to 17.99 s for the DBSCAN-based approach with *MinPts* optimisation and 19.30 s for Hierarchical-based AOMA).

Table 2
Comparison between the eigenfrequencies (left) and the damping ratios (right) as estimated from Acquisition 43A08 (undamaged scenario) and the values reported in [46] for unspecified structural conditions.

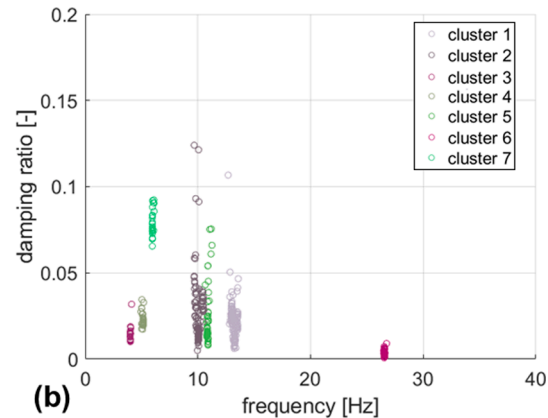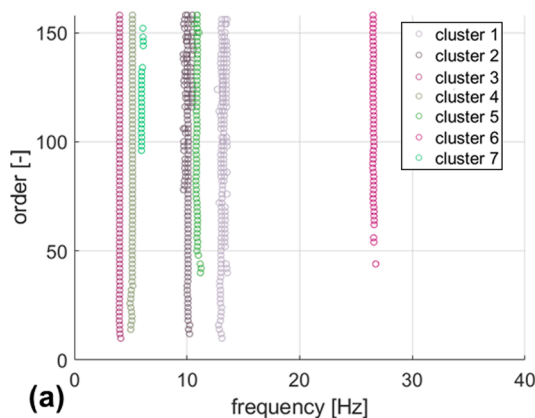|	DBSCAN-based, Acquisition 03B01 [Hz] (difference from target)	Target values [46] [Hz]		DBSCAN-based, Acquisition 03B01 [-] (difference from target)	Target values [46] [-]
f_1	4.02 (+3.85 %)	3.87	ξ_1	0.012 (+34.44%)	0.009
f_2	5.14 (+6.57 %)	4.82	ξ_2	0.022 (+26.88%)	0.017
f_3	5.99 (−10.89 %)	6.72	ξ_3	0.079 (+107.63%)	0.038
f_4	n.a.	8.36	ξ_4	n.a.	0.094
f_5	10.06 (+2.95 %)	9.77	ξ_5	0.025 (+54.06%)	0.016
f_6	10.89 (+3.71 %)	10.50	ξ_6	0.022 (+58.57%)	0.014
f_7	12.26 (-1.29 %)	12.42	ξ_7	0.045 (+41.41%)	0.032
f_8	13.20 (-0.08 %)	13.21	ξ_8	0.022 (-52.84%)	0.047
f_9	n.a.	17.52	ξ_9	n.a.	0.036
f_{10}	n.a.	19.27	ξ_{10}	n.a.	0.025
f_{11}	n.a.	19.65	ξ_{11}	n.a.	0.055
f_{12}	26.54 (-0.38 %)	26.64	ξ_{12}	0.039 (+25.55%)	0.031
f_{13}	n.a.	33.18	ξ_{13}	n.a.	0.043
f_{14}	n.a.	37.25	ξ_{14}	n.a.	0.039

Fig. 8. Modes identified from the undamaged structure (Acquisition 03B01). (a): stabilisation diagram; (b): damping vs frequency diagram.

Hence, both cases (with and without *MinPts* optimisation) overperform the classic hierarchical clustering-based AOMA. Nevertheless, this is not mainly due to the difference between hierarchical and density-based clustering. The most relevant contribution is made by the additional steps of the first case (2-means clustering between possibly physical and certainly spurious poles and outlier removal). The three non-optimised algorithms were run under similar conditions on MatLab® R2020b, using an Intel® Core™ i7-7700HQ CPU with a 2.80 GHz base frequency. Please consider, however, that processing time is a relative metric and depends on the actual implementation and the specific software and hardware.

5.7. Use in damage assessment and comparison with state-of-the-art procedures.

As mentioned in the previous section, it is possible to directly compare the values of the identified natural frequencies and damping ratios with the estimates reported in [20].

Even if the dates corresponding to the reported results are not explicitly stated in this original document, it is evident that these refer to the most damaged conditions. For this reason, their results (obtained by analysing nine different setups and identifying six common modes, deemed as representative of the structure) are here compared with the estimates obtained from the last acquisition (43A08). The identified values show strong similarities (see Table 3). The modes are numbered according to the list provided by [46] and already utilised in Table 2. As previously said, the second and third lateral modes, as well as all modes above 14 Hz, were not reported by [20].

Moreover, to directly establish the contribution of the density-based clustering approach, the results obtained by applying the algorithm described in [23] on the same recording are here included as well. This

hierarchical clustering-based alternative applies the same HVC and SVC, hence, the intermediate results are identical before the application of DBSCAN.

One can see that the values reported in Table 3 represent a noticeable shift from their counterparts presented in Table 2. This variation is graphically portrayed in Fig. 9. As can be seen, some decreases are noticeable in four natural frequencies of interest (Δf_1 = -3.23%; Δf_2 = -7.59%; Δf_5 = -1.79%; and Δf_6 = -4.78%). Apart from the fifth mode, all the other shifts exceeded 3% of the original value. This can be seen as a good indicator of occurring damage. Smaller variations cannot be unequivocally related to it as they can be due to statistical fluctuations of the material properties [49]. Conversely, the two remaining higher modes increase (Δf_7 = + 0.65% and Δf_8 = + 2.05%). Neither of these two, however, seems to indicate a statistically relevant deviation according to the 3% threshold considered above.

Overall, this validates the use of the proposed algorithm for frequency-based damage detection (FBDD). The damping ratios, on the other hand, are supposed to increase with the occurrence of damage [50]. However, this is well-known to be a much less reliable damage index [51], especially for large and complex systems. In the case investigated here, an upward trend can be seen for the first ($\Delta \xi_1$ = + 7.44%), sixth ($\Delta \xi_6$ = + 12.61%), and eighth modes ($\Delta \xi_8$ = + 57.89%). However, an inverse behaviour is evident for the second mode ($\Delta \xi_2$ = -2.64%) and especially for the fifth and seventh ones ($\Delta \xi_5$ = -47.26% and $\Delta \xi_7$ = -42.54%). This confirms the limitations of $\Delta \xi$ as a damage-sensitive feature for bridge monitoring [16].

5.8. Effectiveness under changing environmental conditions.

It is well-known that damage-unrelated phenomena, such as changing environmental and boundary conditions, can significantly affect the modal parameters of concrete bridges, altering their expected response under damaged conditions [52,53]. In particular, temperature-induced frequency shifts can largely exceed damage-induced effects [54]. Thus, on the one hand, the effects of temperature changes should be adequately considered and (if possible) compensated in the results. In this regard, it has been proved in the scientific literature [1] that permanent monitoring systems can be complemented with temperature sensors, to compensate for the large influence of the temperature on the natural frequency estimates. In absence of dedicated sensors, a possible solution is described e.g. in [55]. On the other hand, the precise estimation of these fluctuations is strongly required for any AOMA procedure, independently of its specific application.

To this aim, the evolution of four natural frequencies of interest is plotted in Fig. 10, as a function of time from the 1st till the 250th day of monitoring. The black lines are the original estimates as reported by [41]. Those results are limited to the 3–13 Hz frequency range, which encompasses the four main modes (i.e. the first bending, the fist lateral, and the two mixed bending-torsion ones). Therefore, for consistency, only these modes are considered here as well; the coloured dots represent the eigenfrequencies obtained with the DBSCAN-based AOMA algorithm. The corresponding natural frequencies and damping ratios are reported in Table 4 (except for the first point on day 13, which was already presented in Table 2).

The Z24 bridge underwent several different weather conditions throughout its year-long monitoring. Indeed, this dataset is well-known not only for the damage artificially inserted into its pier but also for the different environmental conditions encountered throughout the whole monitoring period. The most significant effect was cold-induced stiffening, which resulted in time-limited increases in the natural frequencies. The most relevant event happened from 20 January 1998 to 13 February 1998, with a prolonged acute freezing event. As can be seen, the several acquisitions considered here match well both this major and some other minor freezing events.

Clearly, for all acquisitions, the four eigenfrequencies included in the range of interest reported by [41] are correctly identified with the
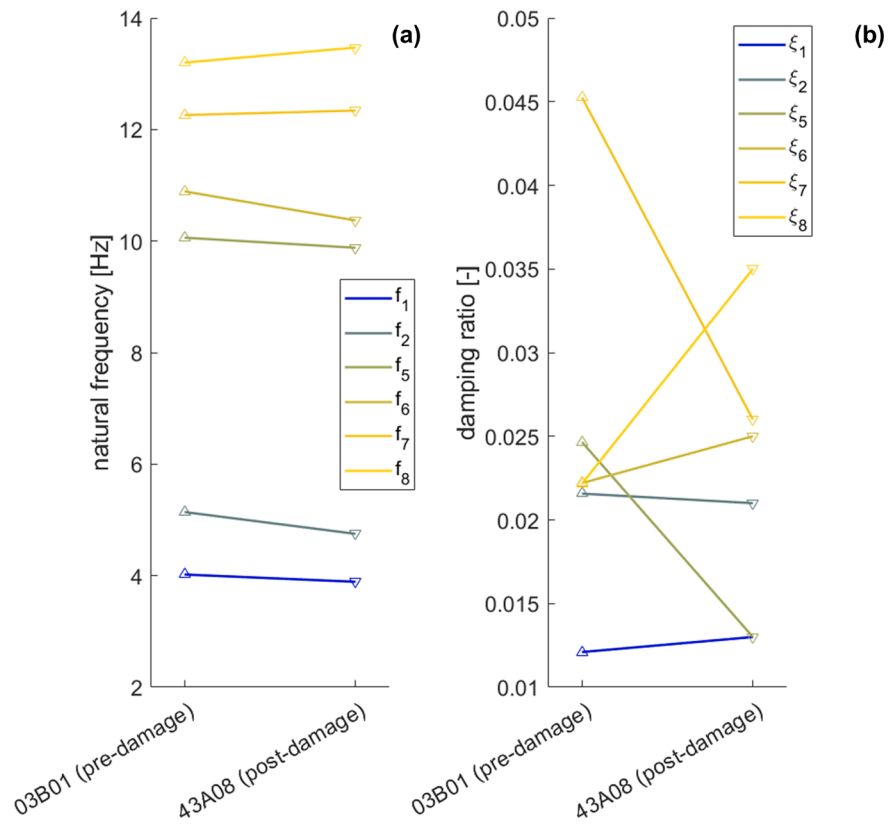
Table 3

Comparison between the eigenfrequencies (top) and the damping ratios (bottom) estimated from applying the DBSCAN-based and the Hierarchical Clustering-based algorithms on Acquisition 43A08 (damaged scenario), benchmarked against the values reported in [20].

	DBSCAN-based, Acquisition 43A08 [Hz] (difference from target)	Hierarchical clustering, Acquisition 43A08 [Hz] (difference from target)	Target values [20] [-]
f_1	3.89 (+0.78%)	3.89 (+0.78%))	3.86
f_2	4.75 (-3.06%)	4.74 (-3.27%)	4.90
f_5	9.88 (+1.23%)	9.89 (+1.33%)	9.76
f_6	10.37 (+0.68%)	10.39 (+0.87%)	10.30
f_7	12.34 (-0.56%)	12.34 (-0.56%)	12.41
f_8	13.47 (+1.89%)	13.47 (+1.89%)	13.22
	DBSCAN-based, Acquisition 43A08 [-] (difference from target)	Hierarchical Clustering, Acquisition 43A08 [-] (difference from target)	Target values [20] [-]
ξ_1	0.013 (+62.50%)	0.013 (+62.50%)	0.008
ξ_2	0.021 (+50.00%)	0.021 (+50.00%)	0.014
ξ_5	0.013 (-7.14%)	0.015 (+7.14%)	0.014
ξ_6	0.025 (+92.31%)	0.025 (+92.31%)	0.013
ξ_7	0.026 (-7.14%)	0.026 (-7.14%)	0.028
ξ_8	0.035 (+2.94%)	0.031 (-8.82%)	0.034

Fig. 9. Shifts in the natural frequencies and damping ratios from (a) the undamaged (Acquisition 03B01) to (b) the damaged (Acquisition 43A48) scenarios, as identified from the DBSCAN-based AOMA procedure.
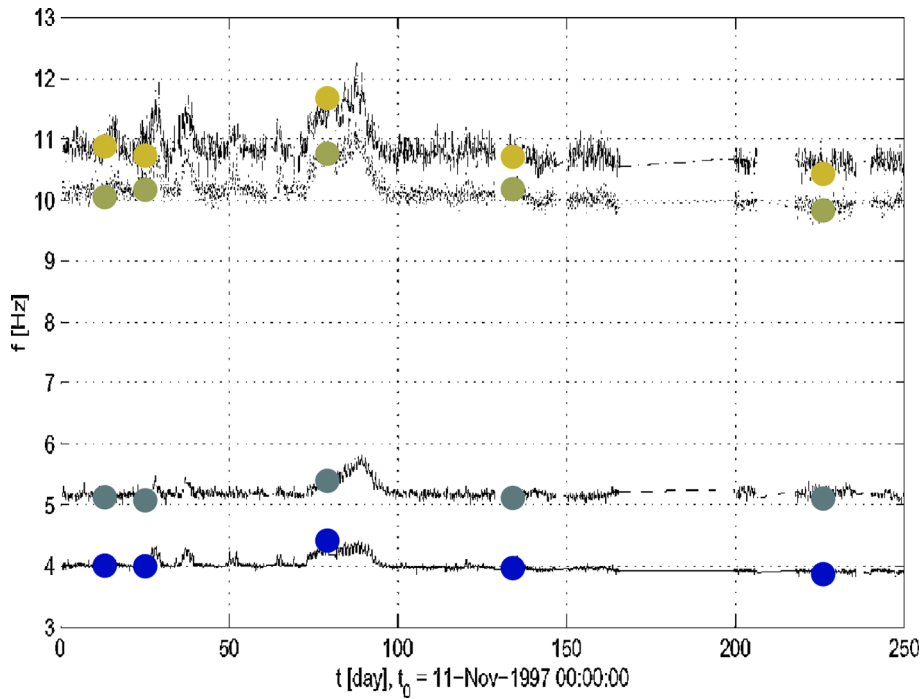

Fig. 10. The frequencies of the four modes considered by [41] from the first till the 250th day of monitoring, compared to the same frequencies as identified with the DBSCAN-based AOMA algorithm (coloured dots).

Table 4
Natural frequencies and damping ratios for the modes of interest and the five recordings (04G18, 12E09, 20D00, 33E11, and 43A08).

	04G18	12E09	20D00	33E11
f_1	4.01	4.43	3.98	3.88
f_2	5.09	5.41	5.13	5.12
f_5	10.18	10.77	10.19	9.84
f_6	10.74	11.68	10.72	10.44
	04G18	**12E09**	**20D00**	**33E11**
ξ_1	0.011	0.010	0.015	0.011
ξ_2	0.032	0.028	0.009	0.022
ξ_5	0.021	0.016	0.015	0.013
ξ_6	0.022	0.023	0.026	0.011

proposed AOMA procedure. That proves its encouraging performances in all weather and environmental conditions.

5.9. Further investigation of the effects of measurement noise

For long-term bridge monitoring, the structural responses are measured under variable operating conditions, resulting in datasets recorded with various noise levels. Hence, it is necessary to prove the robustness of the estimated *MinPts* and ε under such different noise levels. To illustrate the effects of varying noise on the setting of the two parameters (and consequently on the identified outcomes), six cases are considered here. Departing from the experimental acquisition 03B01 (already affected by its actual measurement noise), +0.001%, +0.01%, +0.1%, +1%, +10%, and + 30% additive white Gaussian noise was added (as a percentage of the original signal amplitude). The results are enlisted in Table 5, alongside the identifications from the unaltered signal as previously reported in Table 2. Note that the modes not identified with the unaltered signal are omitted for brevity. As can be seen, *MinPts* does not suffer any variation, even for the highest levels of artificially added noise. ε, on the other hand, increases from 0.0075 to 0.0249 (in particular, more than doubling from + 10% to + 30%). The effects of the more distorted signals can be seen in the results as well. The first bending mode f_1 and the first mixed bending/torsional mode f_5 are both consistently identified for all noise levels, even if with a significant decrease in the accuracy of the estimated damping ratios (largely overestimated in the first case and underestimated in the second one). The first and second lateral modes (f_2 and f_3) are identifiable up to + 10% and + 1% noise respectively, in both cases also with consistent damping estimates. Higher bending and mixed bending-torsion modes, instead, become unidentifiable even with low levels of added noise. Conversely, the pure torsional mode f_{12} remains clearly visible even at + 10%, with quite reliable results in terms of natural frequency and damping ratios.

6. Conclusions

This research dealt with Automated Operational Modal Analysis, proposing a new application for bridge monitoring. The main novelty of the AOMA method discussed here is the inclusion of a fully automatic density-based clustering. That represents a major difference from other pre-existing approaches which rely on hierarchical and ($k = 2$)-means clustering. The details about the similarities and distinctions with other closely-related works have been reported and thoroughly discussed. The experimental evidence – validated on the Z24 case study – confirms what was expected from the DBSCAN theory, that is to say:

- The data points (i.e. the poles) can be easily clustered according to their distance from one another.
- By properly (and automatically) selecting the DBSCAN parameters, the clustering can be limited to the densest areas. Thus, the obtained groups are more likely to correspond to physically meaningful modes. The other, unclustered poles are automatically labelled as spurious and rejected. This property removes the need for a dedicated step to binary classify clusters based on the number of poles included inside them, as it is required instead in the traditional approach with ($k = 2$)-means after hierarchical clustering.
- The density-based approach is naturally capable of recognising and removing outliers in the surroundings of each remaining (physically meaningful) cluster.

Therefore, in comparison to the conventional hierarchical clustering procedure, DBSCAN can perform three tasks at once (grouping similar modes in the cleared stabilisation diagram, selecting the final set of clusters related to physical modes, and removing outliers from the remaining clusters). This application was here fully automated by making the setting of DBSCAN parameters (ε and *MinPts*) data-driven as well, resorting to the Elbow Rule and the Silhouette Index. Future studies will involve the application and validation of this procedure in other compelling structures and infrastructures with different building materials, e.g. long-span cable-stayed bridges.

CRediT authorship contribution statement

Marco Civera: Methodology, Software, Validation, Formal analysis, Investigation, Conceptualization, Writing – original draft, Visualization. **Luigi Sibille:** Methodology, Software, Validation, Visualization. **Luca Zanotti Fragonara:** Conceptualization, Supervision, Project administration. **Rosario Ceravolo:** Conceptualization, Writing – review &

Table 5
Trends of *MinPts, ε,* and the identified natural frequencies and damping ratios for increasing levels of additive white Gaussian noise. Acquisition 03B01.

		unaltered	+0.001%	+0.01%	+0.1%	+1%	+10%	+30%
estimated DBSCAN parameters	*MinPts*	15	15	15	15	15	15	15
	ε	0.0075	0.0075	0.0076	0.0102	0.0109	0.0110	0.0249
first pure bending mode	f_1	4.02	4.02	4.01	4.01	4.01	4.02	4.59
	ξ_1	0.012	0.012	0.012	0.016	0.013	0.013	0.020
first lateral mode	f_2	5.14	5.14	5.14	5.14	5.14	5.14	n.a.
	ξ_2	0.022	0.022	0.021	0.022	0.022	0.021	
second lateral mode	f_3	5.99	5.99	5.98	5.98	6.09	n.a.	n.a.
	ξ_3	0.079	0.079	0.079	0.069	0.077		
first bending-torsion mode	f_5	10.06	10.06	10.06	10.07	10.06	10.06	10.05
	ξ_5	0.025	0.023	0.021	0.025	0.020	0.018	0.014
second bending-torsion mode	f_6	10.89	10.89	10.90	n.a.	n.a.	n.a.	n.a.
	ξ_6	0.022	0.022	0.022				
second pure bending mode	f_7	12.26	12.25	n.a.	n.a	n.a	n.a	n.a
	ξ_7	0.045	0.037					
third pure bending mode	f_8	13.20	13.12	13.02	n.a.	n.a.	n.a.	n.a.
	ξ_8	0.022	0.028	0.027				
pure torsional mode	f_{12}	26.54	26.54	26.53	26.56	26.57	26.50	n.a.
	ξ_{12}	0.039	0.040	0.040	0.039	0.040	0.033	

editing, Supervision, Project administration.

Declaration of Competing Interest

The authors declare that they have no known competing financial interests or personal relationships that could have appeared to influence the work reported in this paper.

Data availability

The Z24 data were collected within the Brite EuRam Programme BE-3157 SIMCES and kindly provided by the project coordinator, the Structural Mechanics Section of KU Leuven.

Acknowledgements

References

[1] C. Rainieri, G. Fabbrocino, Development and validation of an automated operational modal analysis algorithm for vibration-based monitoring and tensile load estimation, Mech. Syst. Signal. Process 60 (Aug. 2015) 512–534, https://doi.org/10.1016/j.ymssp.2015.01.019.

[2] M. He, P. Liang, Y. Wang, Z. li Xia, X. yang Wu, Online automatic monitoring of abnormal vibration of stay cables based on acceleration data from structural health monitoring, Measurement, vol. 195, p. 111102, May 2022, doi: https://doi.org/10.1016/J.MEASUREMENT.2022.111102.

[3] R. Lado-Roigé, J. Font-Moré, M.A. Pérez, Learning-based video motion magnification approach for vibration-based damage detection, Measurement 206 (Jan. 2023), 112218, https://doi.org/10.1016/J.MEASUREMENT.2022.112218.

[4] Y. Wu, S. Li, Damage degree evaluation of masonry using optimized SVM-based acoustic emission monitoring and rate process theory, Measurement 190 (Feb. 2022), 110729, https://doi.org/10.1016/J.MEASUREMENT.2022.110729.

[5] U.M.N. Jayawickrema, H.M.C.M. Herath, N.K. Hettiarachchi, H.P. Sooriyaarachchi, J.A. Epaarachchi, Fibre-optic sensor and deep learning-based structural health monitoring systems for civil structures: A review, Measurement 199 (Aug. 2022), 111543, https://doi.org/10.1016/J.MEASUREMENT.2022.111543.

[6] R. Soman, J.M. Kim, S. Aiton, K. Peters, Guided waves based damage localization using acoustically coupled optical fibers and a single fiber Bragg grating sensor, Measurement 203 (Nov. 2022), 111985, https://doi.org/10.1016/J.MEASUREMENT.2022.111985.

[7] A. Lay-Ekuakille, G. Vendramin, A. Trotta, Spectral analysis of leak detection in a zigzag pipeline: A filter diagonalization method-based algorithm application, Measurement 42 (3) (Apr. 2009) 358–367, https://doi.org/10.1016/J.MEASUREMENT.2008.07.007.

[8] G. Dinardo, L. Fabbiano, G. Vacca, A. Lay-Ekuakille, Vibrational signal processing for characterization of fluid flows in pipes, Measurement 113 (Jan. 2018) 196–204, https://doi.org/10.1016/J.MEASUREMENT.2017.06.040.

[9] M.A. Ugwiri, I. Mpia, A. Lay-Ekuakille, Vibrations for fault detection in electric machines, IEEE. Instrum. Meas. Mag 23 (1) (Feb. 2020) 66–72, https://doi.org/10.1109/MIM.2020.8979527.

[10] M.A. Ugwiri, M. Carratu, A. Pietrosanto, V. Paciello, A. Lay-Ekuakille, Vibrations measurement and current signatures for fault detection in asynchronous motor, in: I2MTC 2020 - International Instrumentation and Measurement Technology Conference, Proceedings, May 2020, doi: https://doi.org/10.1109/I2MTC43012.2020.9128433.

[11] C.R. Farrar, et al., "Dynamic characterization and damage detection in the I-40 bridge over the Rio Grande", Los Alamos, NM (Jun. 1994), https://doi.org/10.2172/10158042.

[12] M.J. Whelan, M.V. Gangone, K.D. Janoyan, R. Jha, Operational modal analysis of a multi-span skew bridge using real-time wireless sensor networks:, https://doi.org/10.1177/1077546310373058, vol. 17, no. 13, pp. 1952–1963, Dec. 2010, doi: https://doi.org/10.1177/1077546310373058.

[13] O.S. Bursi, A. Kumar, G. Abbiati, R. Ceravolo, Identification, model updating, and validation of a steel twin deck curved cable-stayed footbridge, Computer-Aid. Civ. Infrastruct. Eng. 29 (9) (Oct. 2014) 703–722, https://doi.org/10.1111/mice.12076.

[14] Q. Sun, W.J. Yan, W.X. Ren, L.L. Liu, Application of transmissibility measurements to operational modal analysis of railway, highway, and pedestrian cable-stayed bridges, Measurement 148 (Dec. 2019), 106880, https://doi.org/10.1016/J.MEASUREMENT.2019.106880.

[15] Y.C. Ni, M.M. Alamdari, X.W. Ye, F.L. Zhang, Fast operational modal analysis of a single-tower cable-stayed bridge by a Bayesian method, Measurement 174 (Apr. 2021), 109048, https://doi.org/10.1016/J.MEASUREMENT.2021.109048.

[16] M. Civera, V. Mugnaini, L. Zanotti Fragonara, Machine Learning-Based Automatic Operational Modal Analysis: A Structural Health Monitoring Application to Masonry Arch Bridges, Struct. Control. Health. Monit 29 (10) (Jun. 2022) e3028.

[17] F. Magalhães, Á. Cunha, Explaining operational modal analysis with data from an arch bridge, Mechanical Systems and Signal Processing, vol. 25, no. 5. Academic Press, pp. 1431–1450, Jul. 01, 2011. doi: https://doi.org/10.1016/j.ymssp.2010.08.001.

[18] M. Döhler, F. Hille, L. Mevel, W. Rücker, Structural health monitoring with statistical methods during progressive damage test of S101 Bridge, Eng. Struct 69 (Jun. 2014) 183–193, https://doi.org/10.1016/J.ENGSTRUCT.2014.03.010.

[19] R.J. Allemang, Vibrations: Experimental Modal Analysis. University of Cincinnatti, 1999.

[20] E. Reynders, J. Houbrechts, G. De Roeck, Fully automated (operational) modal analysis, Mech. Syst. Signal. Process 29 (2012) 228–250, https://doi.org/10.1016/j.ymssp.2012.01.007.

[21] M.L. Pecorelli, R. Ceravolo, R. Epicoco, An Automatic Modal Identification Procedure for the Permanent Dynamic Monitoring of the Sanctuary of Vicoforte, Int. J. Architect. Heritage 14 (4) (Apr. 2018) 630–644, https://doi.org/10.1080/15583058.2018.1554725.

[22] E. Neu, F. Janser, A.A. Khatibi, A.C. Orifici, Fully Automated Operational Modal Analysis using multi-stage clustering, Mech. Syst. Signal. Process 84 (Feb. 2017) 308–323, https://doi.org/10.1016/j.ymssp.2016.07.031.

[23] V. Mugnaini, L. Zanotti Fragonara, M. Civera, A Machine Learning Approach for Automatic Operational Modal Analysis, Mech. Syst. Signal. Process 170 (2022), https://doi.org/10.1016/j.ymssp.2022.108813.

[24] J. Hair, Multivariate Data Analysis, Pearson Education Limited, 2009.

[25] M. Ester, H.-P. Kriegel, J. Sander, X. Xu, A Density-Based Algorithm for Discovering Clusters in Large Spatial Databases with Noise, in: The Second International Conference On Knowledge Discovery And Data Mining, Aug. 1996.

[26] E.M. Tronci, M. de Angelis, R. Betti, V. Altomare, Multi-stage semi-automated methodology for modal parameters estimation adopting parametric system identification algorithms, Mech. Syst. Signal. Process 165 (Feb. 2022), 108317, https://doi.org/10.1016/J.YMSSP.2021.108317.

[27] E. Reynders, G. De Roeck, Vibration-Based Damage Identification: The Z24 Bridge Benchmark, Encyclopedia Earthquake Eng. (2015), https://doi.org/10.1007/978-3-642-36197-5_72-1.

[28] R. Ceravolo, M. Asce, G. Abbiati, Time Domain Identification of Structures: Comparative Analysis of Output-Only Methods, 2013, doi: https://doi.org/10.1061/(ASCE)EM.1943.

[29] P. Van Overschee, B. De Moor, Subspace Identification for Linear Systems: Theory and Implementation - Applications. Dordrecht: Kluwer Academic Press, 1996.

[30] E. Reynders, G. De Roeck, Reference-based combined deterministic-stochastic subspace identification for experimental and operational modal analysis, Mech. Syst. Signal. Process 22 (3) (Apr. 2008) 617–637, https://doi.org/10.1016/j.ymssp.2007.09.004.

[31] A. Cabboi, F. Magalhães, C. Gentile, Á. Cunha, Automated modal identification and tracking: Application to an iron arch bridge, Struct. Control. Health. Monit 24 (1) (Jan. 2017) e1854.

[32] G.V. Demarie, D. Sabia, A machine learning approach for the automatic long-term structural health monitoring, Struct Health Monit, p. 147592171877919, Jun. 2018, doi: https://doi.org/10.1177/1475921718779193.

[33] A.W. Phillips, R.J. Allemang, Application of modal scaling to the pole selection phase of parameter estimation, Struct. Dynamics 3 (2011) 499–518.

[34] R.J. Allemang, D.L. Brown, A correlation coefficient for modal vector analysis, in: Proceedings of the 1st international modal analysis conference (IMAC 1982), 1982, pp. 110–116.

[35] G.E.P. Box, D.R. Cox, An Analysis of Transformations, J. Royal Statistical Soc:. Series. B. (Methodological) 26 (2) (Jul. 1964) 211–243, https://doi.org/10.1111/j.2517-6161.1964.tb00553.x.

[36] H.K. Seifoddini, Single linkage versus average linkage clustering in machine cells formation applications, Comput. Ind. Eng 16 (3) (Jan. 1989) 419–426, https://doi.org/10.1016/0360-8352(89)90160-5.

[37] S. Aranganayagi, K. Thangavel, Clustering categorical data using silhouette coefficient as a relocating measure, in: International Conference on Computational Intelligence and Multimedia Applications (ICCIMA 2007), 2007.

[38] J. Sander, M. Ester, H.P. Kriegel, X. Xu, Density-Based Clustering in Spatial Databases: The Algorithm GDBSCAN and Its Applications, Data Mining and Knowledge Discovery 1998 2:2, vol. 2, no. 2, pp. 169–194, 1998, doi: https://doi.org/10.1023/A:1009745219419.

[39] E. Schubert, J. Sander, M. Ester, H.P. Kriegel, X. Xu, DBSCAN Revisited, Revisited: Why and How You Should (Still) Use DBSCAN, ACM Trans. Database Syst. (TODS), vol. 42, no. 3, Jul. 2017, doi: https://doi.org/10.1145/3068335.

[40] L. Sibille, M. Civera, L. Zanotti Fragonara, R. Ceravolo, Automated Operational Modal Analysis of a Helicopter Main Rotor Blade with a Density-based Cluster Algorithm, AIAA J. (2022), https://doi.org/10.2514/1.J062084.

[41] B. Peeters, G. De Roeck, One-year monitoring of the Z24-Bridge: environmental effects versus damage events, Earthq. Eng. Struct. Dyn 30 (2) (Feb. 2001) 149–171, https://doi.org/10.1002/1096-9845(200102)30:2<149::AID-EQE1>3.0.CO;2-Z.

[42] J. Maeck, G. De Roeck, Description of Z24 Benchmark, Mech. Syst. Signal. Process 17 (1) (Jan. 2003) 127–131, https://doi.org/10.1006/MSSP.2002.1548.

[43] G. De Roeck, The state-of-the-art of damage detection by vibration monitoring: the SIMCES experience, J. Struct. Control 10 (2) (Apr. 2003) 127–134, https://doi.org/10.1002/STC.20.

[44] J. Maeck, G. De Roeck, Damage assessment using vibration analysis on the Z24-bridge, Mech. Syst. Signal. Process 17 (1) (Jan. 2003) 133–142, https://doi.org/10.1006/MSSP.2002.1550.

[45] A. Teughels, G. De Roeck, Structural damage identification of the highway bridge Z24 by FE model updating, J. Sound. Vib. 278 (3) (Dec. 2004) 589–610, https://doi.org/10.1016/J.JSV.2003.10.041.

[46] E. Reynders, G. De Roeck, Continuous Vibration Monitoring and Progressive Damage Testing on the Z24 Bridge, in: Encyclopedia of Structural Health Monitoring, Chichester, UK: John Wiley & Sons, Ltd, 2008.

[47] N.M. Apaydin, Y. Kaya, E. Şafak, H. Alçik, Vibration characteristics of a suspension bridge under traffic and no traffic conditions, Earthq. Eng. Struct. Dyn 41 (12) (Oct. 2012) 1717–1723, https://doi.org/10.1002/EQE.1196.

[48] R. Ceravolo, N. Tondini, G. Abbiati, A. Kumar, Dynamic characterization of complex bridge structures with passive control systems, Struct. Control. Health. Monit 19 (4) (Jun. 2012) 511–534, https://doi.org/10.1002/STC.450.

[49] M. Civera, M. Ferraris, R. Ceravolo, C. Surace, R. Betti, The Teager-Kaiser Energy Cepstral Coefficients as an Effective Structural Health Monitoring Tool, Appl. Sci. 9 (23) (Nov. 2019) 5064, https://doi.org/10.3390/app9235064.

[50] R.O. Curadelli, J.D. Riera, D. Ambrosini, M.G. Amani, Damage detection by means of structural damping identification, Eng. Struct 30 (12) (Dec. 2008) 3497–3504, https://doi.org/10.1016/j.engstruct.2008.05.024.

[51] E. Reynders, R. Pintelon, G. de Roeck, Uncertainty bounds on modal parameters obtained from stochastic subspace identification, Mech. Syst. Signal. Process 22 (4) (May 2008) 948–969, https://doi.org/10.1016/j.ymssp.2007.10.009.

[52] M. Dilena, A. Morassi, Dynamic testing of a damaged bridge, Mech. Syst. Signal. Process 25 (5) (Jul. 2011) 1485–1507, https://doi.org/10.1016/J.YMSSP.2010.12.017.

[53] M. Dilena, A. Morassi, M. Perin, Dynamic identification of a reinforced concrete damaged bridge, Mech. Syst. Signal. Process 25 (8) (Nov. 2011) 2990–3009, https://doi.org/10.1016/J.YMSSP.2011.05.016.

[54] M.P. Limongelli, Frequency response function interpolation for damage detection under changing environment, Mech. Syst. Signal. Process 24 (8) (Nov. 2010) 2898–2913, https://doi.org/10.1016/J.YMSSP.2010.03.004.

[55] C. Surace, A. Bovsunovsky, The use of frequency ratios to diagnose structural damage in varying environmental conditions, Mech. Syst. Signal. Process 136 (Feb. 2020), 106523, https://doi.org/10.1016/j.ymssp.2019.106523.